# Synthesis and Experimental-Modelling Evaluation of Nanoparticles Movements by Novel Surfactant on Water Injection: An Approach on Mechanical Formation Damage Control and Pore Size Distribution

***Parvazdavani, Mohammad***
*Upstream Faculty, Research Institute of Petroleum Industry (RIPI), P.O. Box. 1485733111 Tehran, I.R. IRAN*

***Kiani, Sajad***
*Material Engineering, Swansea University, Singleton Park, Swansea SA2 8PP Wales, UNITED KINGDOM*

***Abbasi, Saeed****[+]
*Upstream Faculty, Research Institute of Petroleum Industry (RIPI), P.O. Box. 1485733111, Tehran, I.R. IRAN*

**ABSTRACT:** *Water injection is used as a widespread IOR/EOR method and promising formation damages (especially mechanical ones) is a crucial challenge in the near-wellbore of injection wells. The magnesium oxide (MgO) NanoParticles (NPs) considered in the article underwater flooding experiment tests to monitor the promising mechanical formation damage (size exclusion) in lab mechanistic scale include micro-scale classical deep bed filtration model, permeability, and pore size distribution. The averaged upper-scale equations were constructed on the water injection basis on the presence of NPs. The model validation to adjust the equation of state was obtained based on fluid samples from the laboratory and simulation tests. The permeability decline (up to 50% initial permeability) was important when the optimum value of capturing the probability coefficient ($p_a$) is 0.7 mismatched on the conventional simulation results. Pore size distribution in each simulation time step based on retention concentrations determined in the sandstone samples. Formation damage analyses on the presence of NPs showed that modification of the static reservoir models has excellent potential regarding porosity and permeability maps, in large-scale simulation. This study displays an improved approach to NPs' movement through a porous medium which will act as a benchmark for future waterflooding EOR projects in sandstone oil reservoirs or similar basins all over the world.*

**KEYWORDS:** *Water Injection; Formation Damage; Particle Movement; Water Flooding; Permeability Reduction*

***** *To whom correspondence should be addressed.*
*+ E-mail: abbasis@ripi.ir*
*1021-9986/2020/1/209-223* *15/$/6.05*

## INTRODUCTION

The purpose of Enhanced Oil Recovery (EOR) is to increase the amount of oil recovery throughout the porous media. Water can be injected into sandstone and carbonated reservoirs with different geographical structures, which can result in several problems. These include mixtures of injection and reservoir water flowing at various temperatures and pressures, inefficient recovery due to variable permeability of porous media (heterogeneity), and early water breakthrough and as a result of formation damage [1-3]. Over the last few decades, different methods for avoiding formation damage have been put into action [4-13]. Reducing formation permeability is usually achieved by pore blockage of reservoir rock and the fast movement of particles (fines migration) [14-16]. Many researchers have found that permeability impairment causes reduction in both injection and productivity indexes [4, 17]. Moreover, in some cases, water injection decreases injectivity due to the poor quality of water and suspended particles in produced water near the wellbore region [18, 20, 48]. These facts prompted scientists to set up laboratory and modelling reservoir formation tests to study the water flooding for impaired formation damage via particle movements in oil reservoirs. Various clay stabilizers have been suggested for clay migration in the presence of different ion concentration such as $Ca^{2+}$, $Mg^{2+}$, $Cl^{-}$ with several additives for particle fine migration such as amine-based choline chloride, tetramethyl ammonium choloride, Al/Zr-based stabilizers, and nanoparticles [19, 20]. Recently, smart fluids or nanofluids (a colloidal suspension of nanoparticles) are used to enhance the oil recovery because of two main characteristics of nanoparticles (1) their size and (2) the ability to manipulate their behavior. Small sizes of the dispersed phases leads to large specific surface area and improved flow through typical reservoir pore spaces. Smart fluid flooding basically involves disjoining pressure gradient, IFT reduction, wettability alteration and plugging of pore channels by nanoparticles adsorption [44-47]. In 2006, the hydrophilic polysilicone nanoparticles were used to improve water flooding and fine particle migration in pore throat results, reducing porosity and permeability [21]. Nanofluids result in oil reservoirs showing exclusive properties such as a reduction in wettability alteration, oil viscosity modification, IFT reduction and foam stabilization, all of which prevent fine particle migration [22-24]. Adsorption tendency and superbly modified structures sort them as a suitable candidates on particular purposes [26]. Nanoparticle sizes through interconnected rock pore-throat (μm) has slight effects on damage of pore-reservoir structures and permeability. For the time being, decrease the double layer repulsive forces among particles and rock grains [21, 27]. Formation of stable nanoemulsion with minimal droplet size requires proper selection of HLB value of the emulsifier [26]. The droplet size and stability of emulsion is also affected by the type and concentration of surfactant used. The IFT reduction totally depends upon the amount of surfactant adsorbed at the oil-water interface. Surfactant adsorption is a complex phenomenon where surfactant molecules from the bulk phase are transported at the oil-water interface [47].

A number of mechanisms might be involved in surfactant adsorption such as van der Waals interaction, covalent bonding, electrostatic interaction, hydrogen bonding, etc [30]. Fig. 1 shows an emulsion droplet with surfactant monomers adsorbed.

Furthermore, other studies on hydraulic fracturing procedure have also proved that the slight concentration of nanoparticles coated on proppants can significantly avoid particle fines migration and consequent formation damage [27]. Furthermore, silica nanoparticles as a suitable agent with utilizing nC60 on fine migration treatment have been reported [28]. In conclusion, considering to damage on reservoir formation is involve in unsuitable extraction by chemicals, and flooding methods which are choose for improved oil recovery (IOR/EOR) [28, 29].

The lack of possibility of commercial software to track the size exclusion damage caused by solid particles movement. As observed, due to lack of consideration of PSD in simulation, size exclusion mechanism of mechanical formation damage wasn't monitored in synthetic base case. On the other hand, permeability decline is consequence of modification in pore size distribution of porous medium demanding the application of models including pore size distribution in simulation.

Many studies have been done on formation damage caused by size exclusion mechanism and pore throat plugging [31-34]. *You et al.* developed

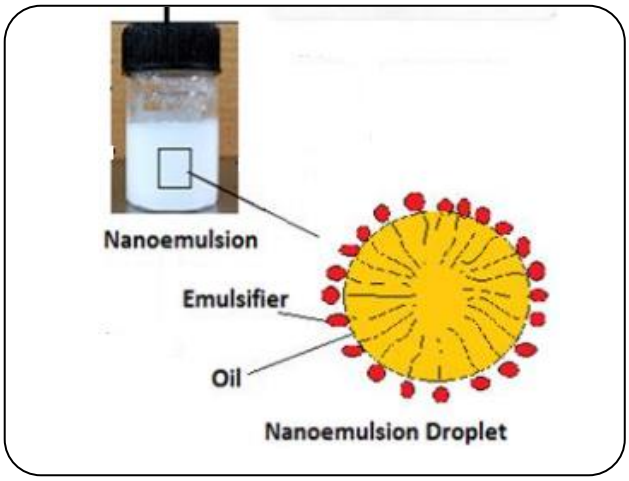


***Fig. 1: Emulsion droplet with surfactant monomers adsorbed.***

the asymptotic model for non-linear deep bed filtration processes and determine the suspension concentration and break through time more accurately by accounting the Pore throat Size Distribution (PSD) effect in flow equations [34]. *Chalk et al.* developed an effective method based on micro scale modelling for determination of overall PSD by injection of colloidal particle suspensions into engineered porous media with monitored inlet and breakthrough particle concentrations [32]. Santos tried to prove that the utilization of micro scale equations for exact up scaling (averaging) in case of filtration of mono dispersed suspensions is accurate and the averaged upper scale equations generalize the classical deep bed filtration model and its latter modifications [37]. He developed a pore scale model, incorporating particle and pore size distributions, and discussed the corresponding averaged equations and applied to predict pore blocking and permeability reduction during dead-end and cross-flow microfiltration in membranes. Farajzadeh studied the extent and mechanism of the damage caused by produced water re-injection. He carried out laboratory experiments in order to investigate and predict the damage. The study was done both on internal filtration and external cake build up [36]. For the internal filtration results, he used the classical deep bed filtration theory and for the external cake build up, a new model was proposed.

In all of the mentioned studies, the probability coefficient was obtained based on the engineered porous medium to produce the results consistent with experimental data. In some of them due to instability of particles in injection water evoked by grain surface charge distribution or gravity (e.g. Positive charged Iron, Heavy bentonite), stable results for comparison couldn't be obtained. These unstable particles caused the immediate deposition of suspended solids within the injecting lines prior to the entrance of porous media or lack of enough stability throughout the porous medium causing the inaccurate estimation of size exclusion effect on formation damage analysis. Based on these two issues, special tests designed for effect of PSD on particles capturing in core sample porous media in order to extract the authentic experimental results consistent with the reservoir condition and obtain more reliable modelling parameters such as capturing probability coefficient.

The pioneering work that covered the lack of application of nanoparticle behaviours in formation damage analysis (specially mineral scale) with the presence of modelling results have been evaluated at this article. In this study, due to lack of possibility of commercial software to simulate the formation damage in core scale, we developed the model and investigate the applicability of modelling results in reservoir conditions. Regarding this issue, stable magnesium oxide NanoParticles (NP) were used to monitor the mechanical formation damage and deep bed filtration theory with tuned parameter was applied for authentic estimation of permeability reduction due to size exclusion.

## EXPERIMENTAL SECTION

### *Experimental Section*

To monitor the size exclusion mechanism of mechanical formation damage in porous media as well as determining the required parameters of model, a precise test has been designed. To prepare the suspended particles in distilled water, MgO nanoparticles are synthesized and their properties are characterized. Then, the nanoparticles are used for mechanical formation damage as a nanofluid with anionic surfactant (accumar-3100) for long-time stabilization of particles in water injection [36].

MgO NPs reduce pore blockage in reservoir rock because; first, lack of deposition possibility with respect to MgO NPs in higher concentration due to aggregation

of nanoparticles [37-39]. Second, the economics of MgO NPs through the mechanical formation damage will also be justified compared to other compounds [40]. Since nanoparticles stick to reservoir surface and change the pore size distribution as well as porosity, type of NPs is crucial. Among the conventional nanoparticle, such as $SiO_2$, and MgO, a spherical structure is required. These spherical NPs do not react with reservoir surface and as a result no rapid agglomeration occurs. As an example, hydroxyl (OH) groups adhere on the surface of $SiO_2$ in sandstone core samples and causes instable flow of particles. Therefore, MgO NPs with surfactant accompanied were used to design the stable experiment.

***Synthesis and Characterization of MgO Nanoparticles***

MgO nanoparticles were synthesized using chemical precipitation method by mixing 0.7 g of $C_9H_{12}O_4S_2$ and 5.5 g Mg $(CH_3COO)$ $2.4H_2O$ in 70 mL DMSO solution under stirring condition at room temperature for 1h. Polyethylene glycol (PEG) (6000, 3.5 g) was then added and refluxed at 90 $^oC$ for 8 h and droplets of aqueous solution of $NH_4OH$ (4M) were added into the solution until pH=8.5. In the next step, the white solution was filtered and washed with distilled water until the pH value reached to 7. Finally, the MgO NPs were dried at 90 $^oC$ in oven and calcined at 500 $^oC$ for 4 h.

Morphological characterization and crystalline structures of MgO were obtained by Field Emission Scanning Electron Microscopy (FESEM, Hitachi S-4160, Japan), Transmission Electron Microscopy (TEM, Zeiss EM-900), and X-Ray Diffraction (XRD meter using the Cu Kα source at 40kV and 40 mA). Also, the image of the MgO NPs in water was examined using an optical microscope (Nikon Eclipse LV100**).** Fig. 2 shows the X-Ray Diffraction (XRD) pattern of the as-synthesized MgO NPs. The diffraction peaks were consistent with the standard pattern of MgO (JCPDS Card No. 87-0653) which can be indexed face-centred cubic phase [41].

Fig. 3.a shows Mg (CH3COO) $2.4H_2O$ which is the precursor for synthesis of MgO in the presences of PEG 6000. The TEM image in Fig. 3.b demonstrates the MgO NPs spherical morphology with different particle size which is produced by chemical precipitation method.

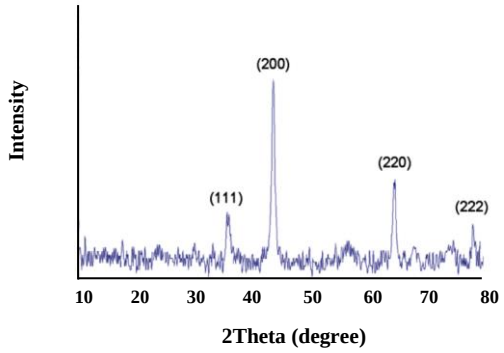


***Fig. 2: X-ray diffraction pattern for synthesized MgO nanoparticle.***

The nanoparticles in this Fig. are in the range of 10-50 nm. Some orders and long-range disorders in spherical particle shapes without aggregation were observed which is confirmed by XRD result.

At mass ratio 1:1 concentration, abundant particles was bound to accumar-3100 and made the MgO NPs very stable in suitable size. At low surfactant concentration, many fragments of nanoparticles adhered to the surfactant in deionized water. The adhesion suspends the particles of MgO NPs. The MgO NPs were relatively hydrophilic. We used a surfactant to stabilize nanofluid and prepare the required particles with suitable sizes (see Fig. 4 as the proper sized particles). In order to perform the MgO NPs injection, the nanoparticle concentration was set to 0.1 wt. % as the optimum value. The main reason is related to consideration of both lower cost as well as stable solution.

Fig. 5 shows the variation of zeta potential with surfactant concentration. At higher surfactant concentration a slow drop in zeta potential values is observed and tends to become constant. This may be due to complete saturation of surfactant molecules at the NP's-aqueous interface and formation of micelles or globules in solution phase. The surfactant addition results in the formation of stable NP's solution.

***Core Sample Properties***

The sandstone core sample with the diameter of 3.8 cm and pore volume 7.45 mL is used for experimental evaluation (Table 1).

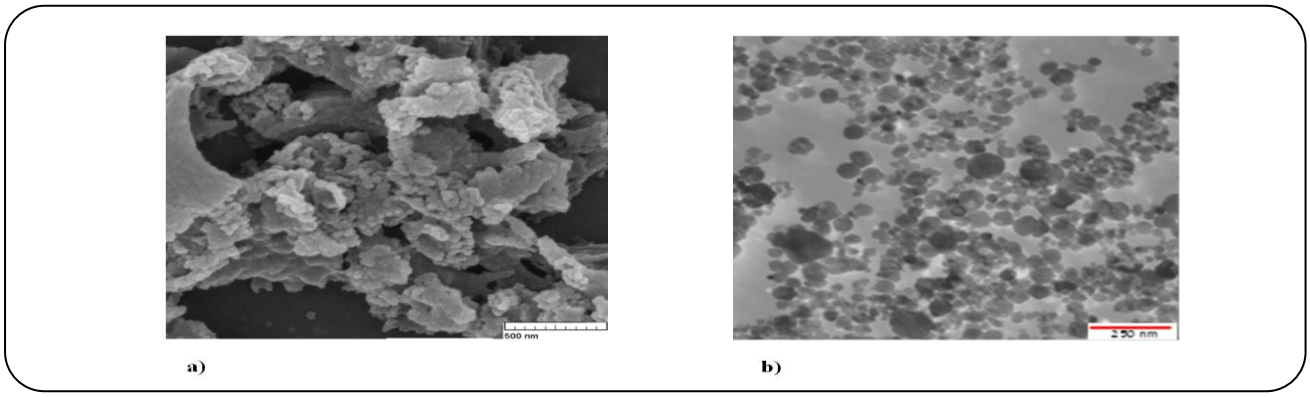


*Fig. 3: a) FESEM image of MgO nanoparticles with addition of PEG 6000. b) TEM image of MgO nanoparticles.*

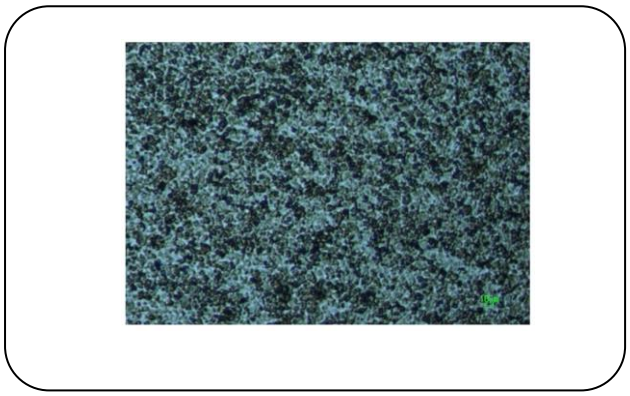

*Fig. 4: SEM image of Stable MgO NPs with optimum 0.1 wt. % nanoparticle concentration.*

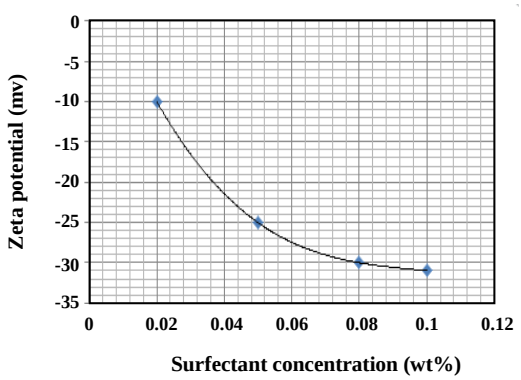


*Fig. 5: Effect of surfactant concentration on zeta potential (mv).*

To monitor size exclusion effect of mechanical formation damage, Pore Size Distribution (PSD) of core sample should be defined as an initial step to design the particle sizes as well as to determine the required parameters for modeling (Fig. 6).

According to stochastic mean value of 3.47 µm for pore sizes in core sample, NPs with distribution of sizes in range of 2-10 µm can be used (Fig.7)

XRD analysis of selected sandstone was shown in Fig. 8. As shown the major constituents of core sample is quartz which didn't react with MgO NPs as the suspended solids.

***Experimental Setup and Procedure***

Fig. 9 shows the schematic of the experimental setup. The setup is mainly consists of a high-pressure positive displacement (DBR) pump for confining different pressure and volumetric flow rate, confining pressure system, transfer vessel, core sample holder situated horizontally which is composed of a steel vessel connected with the confining pressure control system, a back pressure regulator for pressure regulating of fluid in core, and data acquisition record. Prior to the experiments, core sample was washed by toluene, and then the core was solvent cleaned and dried with hot nitrogen and evacuated. After core preparation, the core is saturated by the saturator apparatus with distilled water. Absolute permeability is calculated by Darcy Equation at different injection rates (8, 12 and 18 mL/h) up to pressure drop stabilization. Then, MgO NPs were injected at different flow rates (6, 12, 18, 24 and 36 mL/h) and at pressure (1 atm.). To investigate the effect of flow rate and determine the filtration coefficient dynamically for modelling as well as checking the possibility of deposition due to size exclusion, forward and backward trends of injection rates (i.e. firstly flooding in trend of increasing rates and then decreasing) have been done. The hysteresis of pressure drop curves at each step of injection rates and its consequent effect on mechanical damage was evaluated and indicating the damage qualitatively.

***Table 1: Properties of the Selected Core Sample.***

| | |
|---|---|
| Grain density (gr/cm3) | 2.650 |
| Porosity (%) | 5.114 |
| Length (cm) | 12.985 |
| Brine-Absolute permeability (D) | 1.190 |

The main limitations on experiments are lack of NMR apparatus to track the front dynamically and lack of homogenizer to be certain that we haven't any particles deposition prior to entrance of the rock inlet. First one can be removed by multi pressure transducer apparatus and surfactant can be used to solve the second problem by stabilization on injection NP's.

***Classical Deep Bed Filtration (DBF) theory***

To model the capturing mechanism of particles throughout the porous media in water injection and remove the specified challenge in simulation (Fig. 1), deep bed filtration theory was used to determine the suspension and retention concentrations [34].

The preseneted model is for Darcy flow in 1-D and can't be applied in cases that we have eddy flow. Second, we assume that particles are in spherical rounded shape and didn't use any shape factors. Finally this solution is zero order solution (linear front) of particles and is valid during short after-the breakthrough periods.

Modelling was done based on averaging system leading to evaluation of the suspended fine particles transport in porous media (Eq. (1)) [42].

$$\varnothing_a(\sigma)\frac{\partial c}{\partial t}+U\frac{\partial}{\partial x}\left[cf(\sigma)\right]=-\frac{\partial \sigma}{\partial t} \quad (1)$$

$$\frac{\partial \sigma}{\partial t}=\frac{1}{l}\frac{k_c(\sigma)}{k(\sigma)}Uc$$

$$k_c(\sigma)=\int_0^{\infty}\left[1-\upsilon\left(\frac{r_0}{r_p}\right)+\upsilon p_a\left(\frac{r_0}{r_p}\right)\right]k_1(r_p)H(r_p)dr_p=$$

$$\int_0^{\infty}p\left(\frac{r_0}{r_p}\right)k_1(r_p)H(r_p)dr_p$$

Rate of retention can be shown in form of Eq. (2) in which the proportion coefficient will be shown based on the integration term of Eq. (1).

$$\frac{\partial \sigma}{\partial t}=\lambda' Uc \quad (2)$$

$$\lambda'(\sigma)=\frac{p'}{l},\ p'=\frac{k_c(\sigma)}{k(\sigma)}$$

Where p´ was calculated based on probability of particles attached or trapped throughout the flow path (Eq. 3). This value depends on ($p_a$), the capturing probability coefficient, which can be considered as tuning parameter of developed model.

$$p'=1-f(\sigma)+p_a f(\sigma) \quad (3)$$

When the probability of particle trapping is constant, Eq. (2) can be modified to Eq. (4).

$$\frac{k_c(\sigma)}{k(\sigma)}=1-f(\sigma)+p_a f(\sigma) \quad (4)$$

$$\frac{\partial \sigma}{\partial t}=\frac{1-f(\sigma)+p_a f(\sigma)}{l}Uc$$

Eq. 3 is similar to Bayesian framework for particle trapping probability in porous media model the particle movements by Eq. (5).

$$\frac{\partial \sigma(x,t)}{\partial t}=\lambda_0\left[1-f(r_s,\sigma)\right]Uc(x,t) \quad (5)$$

The filtration coefficient of screening is given by Eq. (6).

$$\lambda_0=\frac{1}{l} \quad (6)$$

Based on definition of suspended saturation ($s=\varphi_a/\varphi$), Eq. 1 can be rewritten as Eq. (7).

$$\varnothing_a(\sigma)s(\sigma)\frac{\partial c}{\partial t}+\frac{\partial}{\partial x}\left[cf(\sigma)\right]=0 \quad (7)$$

Finally, the partial flow model is obtained as Eq. (8).

$$\varnothing_a(\sigma)s(\sigma)\frac{\partial c}{\partial t}+\frac{\partial \sigma}{\partial t}+U\frac{\partial}{\partial x}\left[cf(\sigma)\right]=0 \quad (8)$$

$$\frac{\partial \sigma}{\partial t}=\lambda' Uc$$

$$U=-\frac{k(\sigma)}{\mu}\frac{\partial P}{\partial x}$$

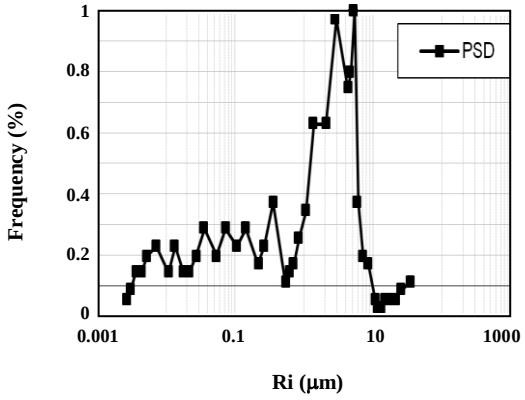


***Fig. 6: Pore size distribution of sandstone core sample.***

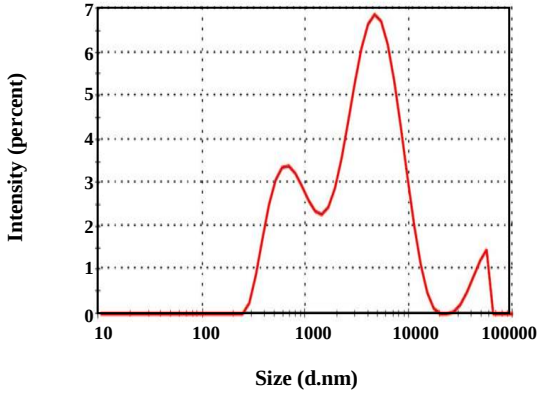


***Fig. 7: Particle Size Distribution (PSD) curve of injected NPs.***

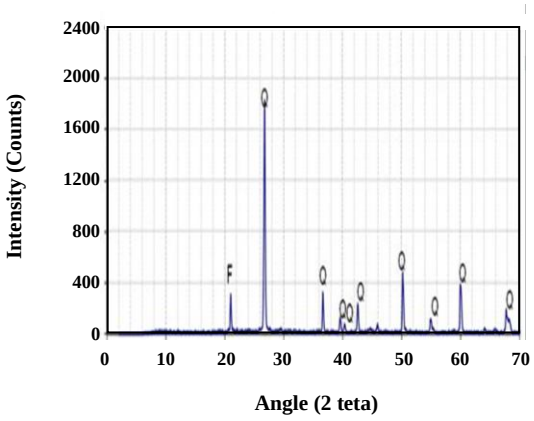


***Fig. 8: X-ray diffraction pattern Curve of Core Sample.***

There are four parameters in Eq. (8) ($\phi(\sigma)$, $f(\sigma)$, $\lambda'(\sigma)$ and $k(\sigma)$). For constant probability coefficient ($p_a$), filtration function can be determined by fractional flow function based on two constants, $p_a$ and l. The first two terms of Eq. (8) will be solved simultaneously to determine C and σ. The last term (Darcy Equation) will be applied to calculate the pressure drop occurred due to capturing. Required functions, $\phi_a(\sigma)$, $f_a(\sigma)$ and $\lambda(\sigma)$ will be determined by Eq. (9).

$$\phi_a(\sigma) = \int_{r_0}^{\infty} \pi r_p^2 H_0(r_p) e^{-k_1(r_p)[1-\nu(j)+\upsilon p_a(j)]y(h_0-l\sigma)} dr_p \qquad (9)$$

$$f_a(\sigma) =$$

$$1/k(\sigma) \int_{r_0}^{\infty} \nu(j) k_1(r_p) H(r_p) e^{-k_1(r_p)[1-\nu(j)+\upsilon p_a(j)]y(h_0-l\sigma)} dr_p$$

$$\lambda(\sigma) = \frac{1}{lk(\sigma)} f_a(\sigma) \int_0^{\infty} [1-\nu(j)+\upsilon p_a(j)] \times$$

Where k can be determined by Eq. 10.

$$k(\sigma) = \int_{r_0}^{\infty} k_1(r_p) H_0(r_p) e^{-k_1(r_p)[1-\nu(j)+\upsilon p_a(j)]y(h_0-l\sigma)} dr_p \qquad (10)$$

By obtaining the unknown variables (C and σ), pore size distribution function (H) can be modified dynamically by Eq. 11.

$$H(r_p, x, t) = H(r_p, y(h)) = \qquad (11)$$

$$= H_0(r_0) \int_{r_0}^{\infty} k_1(r_p) H_0(r_p) e^{-k_1(r_p)[1-\nu(j)+\upsilon p_a(j)]y(h_0-l\sigma)} dr_p$$

## RESULTS AND DISCUSSION

There are two main sections of results discussed in following subsections regarding experimental data leading to extraction of required parameters for tuning of modelling section and consequently determination of concentration profiles. All of the indicator curves for investigation in mechanical damage are presented in experimental section.

### *Experimental Results*

The experimental results of Mgo NP injection regarding the pressure drop curves in different

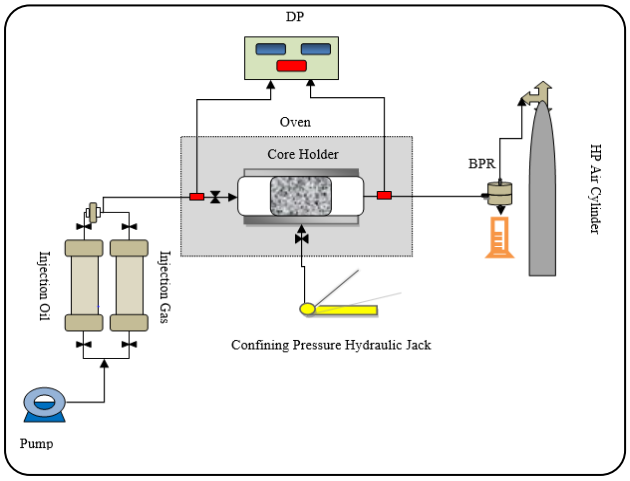


*Fig. 9 Schematic of the experimental setup.*

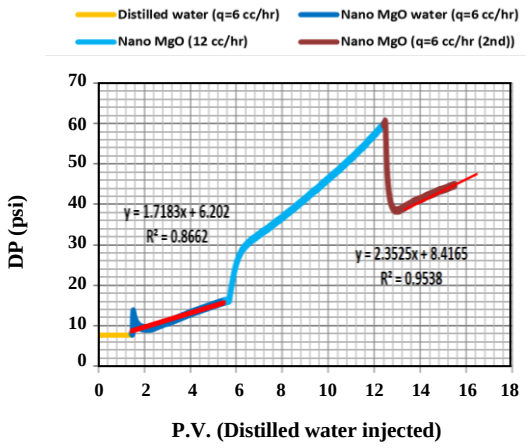


*Fig. 10: Pressure drop curve of MgO nanofluid after injection at different flow rates.*

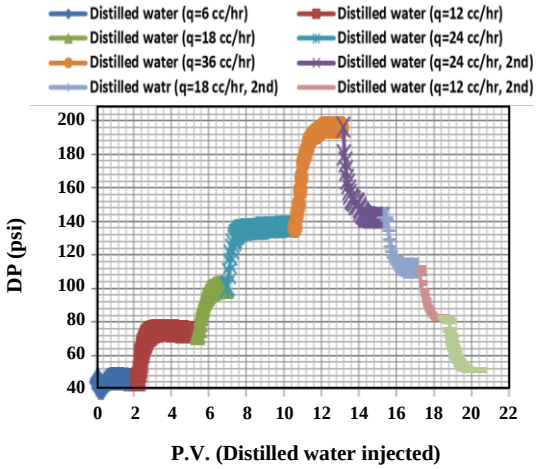


*Fig. 11: Pressure drop curve in different injection rates (forward: rate increasing, backward: rate decreasing).*

scenarios have been shown and finally permeability impairment curve due to damage has been presented.

The results of Mgo NP injection pressure drop for different injection rates were shown in Fig. 10. Due to common range of particle diameter and average pore diameter, the capturing happened and pressure drop increases with increasing slope. There are two main reasons for this increase; firstly increase of injection rate and secondly increase of capturing due to mechanical damage indicating the dependency of retention rate on both of bulk velocity and filtration coefficient [47]. Since the slope of increase at the same injection rate (6mL/h) is not the same (Fig. 10), filtration coefficient was changed dynamically.

The capturing phenomenon can be verified by the hysteresis of pressure drop in cases of forward and backward injection. In this scenario after the Nano fluid injection, distilled water was injected at increasing rates and then continued at decreasing rates. The difference between stabilized pressure drop values at same rates shows the occurred damage in porous medium (Fig. 11) [48].

Another indicator of plugging through the injection process is pressure drop stabilization after NPs injection showed that the size exclusion stopped after the distilled water injection and the previous increase was due to damage (Fig. 12).

To characterize the possible damage of size exclusion mechanism, absolute permeability of core sample curves after and before of NPs injection was calculated by determination of slop of different rate versus stabilized pressure drop shown in Fig. 13. As observed, slope was increased in case of NPs injection indicating the decrease of absolute permeability in order of 3.37.

One of the main aspects in experimental formation damage analysis is to design the stable test. To indicate the validity of test, two tests within and without the use of NPs coated with surfactant were implemented to determine the efficiency of damage (permeability decline) throughout the injection period (Fig. 14). As observed, stabilization of suspended solids in lines prior to inlet of core sample is higher in case of stable MgO NPs injection compared to other one that portrait better experimental investigation of size exclusion mechanism in mechanical formation damage studies.

At low surfactant concentration large droplet size was observed because of a restively high interfacial tension and coalescence of oil droplets, which is supported by a low zeta potential value. With increase in surfactant concentration a decrease in droplet size was observed due to significant increase of interfacial area and reduction of interfacial energy which in turn reduces the interfacial tension denoting less coalescence of oil droplets and increase in stability of emulsion. The increase of ratio of surfactant film thickness to droplet radius due to accumulation of surfactant molecules at the interface provides better stabilization against droplet aggregation and helps in lowering the flocculation rate as well as reduces the droplet size.

Finally effect of rate on intensity of capturing was evaluated and its final output (permeability decline) was presented in different cases of injection rates (Fig. 15).

Fig. 15 shows that, when the injection rate increases the slope of the permeability decline increases. This observation verified by proportional relation of filtration coefficient with bulk velocity.

The hysteresis of PSD (Particle Size Distribution) at effluent of core regarding the injection rate after the retention occurrences was shown in Fig. 16.

As observed, whenever the rate increased share of higher sizes at affluent increased. But decrease of rate from12 mL/h to 6 did not provide the same trend of PSD frequency as observed in first case (6mL/h). This effect is due to detachment of fine particle and their appearance at effluent which was approved by experimental pressure drop curves at different surveys of rates (Fig. 10).

### *Modelling Results*

The modeling study was performed using the input parameters for DBF theory reported in Table 2.

To import the PSD of core sample in governing equation, following fitting equation was used (Fig. 17).

Information of tuned PSD equation is shown in Table 3.

Suspension concentration was shown at outlet and sensitivity analysis was done on capturing probability coefficient ($p_a$) to obtain the most consistent results with experimental measured concentrations at lab scale in different time steps throughout the injection time (Fig. 18).

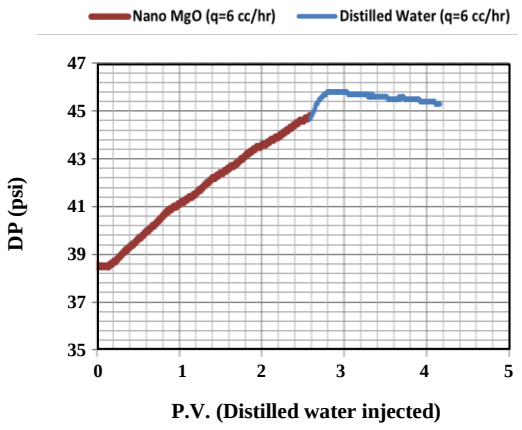


***Fig. 12: Pressure drop stabilization after MgO nanofluid.***

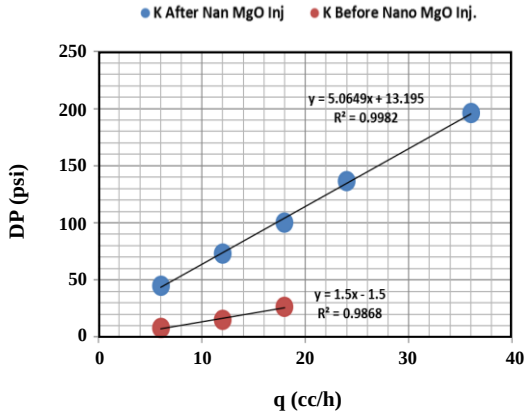


***Fig. 13: Absolute permeability comparison before and after MgO nanofluid injection.***

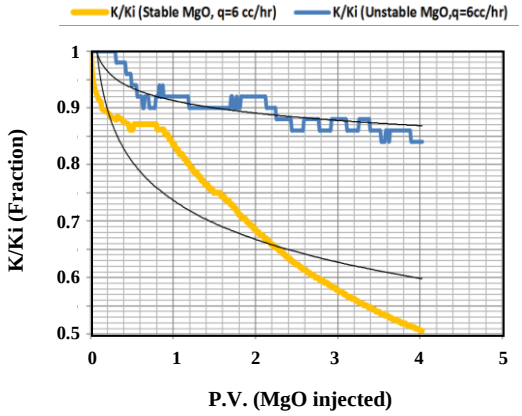


***Fig. 14: Comparison of the permeability reduction curves: MgO NPs by surfactant (Stable) and without surfactant (unstable).***

***Table 2: Input Data of the Selected Core Sample.***

| | |
|---|---|
| Number of grid cells and direction | 16, X |
| Injection rate (cc/min) | 0.1 |
| Distance between pore spaces (μm) | 2.1 |
| Modeling time (P.V) | 10 |

***Table 3: Statistics of fitted equation for the Selected Core Sample PSD.***

| |
|---|
| f(x) = $a_1$*exp.(-((x-$b_1$)/$c_1$)^2) |
| Coefficients (with 95% confidence bounds): |
| $a_1$ = 0.9442 (0.8248, 1.064) |
| $b_1$ = 3.82 (3.554, 4.087) |
| $c_1$ = 2.902 (2.582, 3.223) |
| SSE: 0.3752 |
| R-square: 0.8452 |
| Adjusted R-square: 0.837 |
| RMSE: 0.09937 |

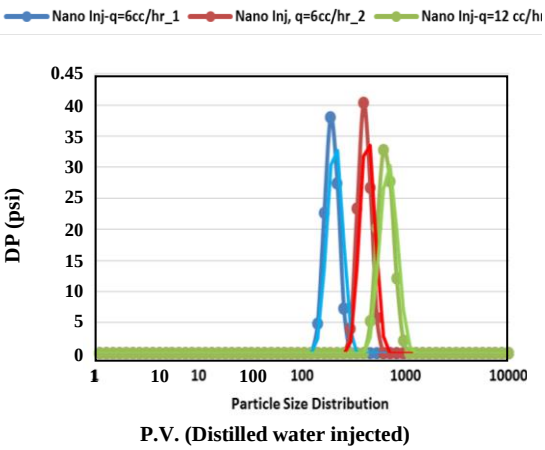


***Fig. 16: Hysteresis curve of particle size distribution at effluent of core versus injection flow rate.***

As observed in Fig. 18, after nearly 0.95 P.V of NPs injection break through occurred and ultimately after more than 3.5 P.V concentration value stabilized and no other particles captured. This behaviour admits the limited capacity of retention concentration proportional to time, velocity and filtration coefficient (Eq. (2)). The specified trend was observed in all other grid cells (Fig. 19).

To investigate the effect of particles size on effluent concentration, simulation was run for different sized (Fig. 20). As observed in cases of particles injections with particle sizes higher and lower than average of porous medium ($r_s$=1.75 and 6.95 μm as 0.5 and 2 times larger than porous medium size), different behaviours of effluent suspension concentration curve was obtained.

This difference in order of magnitude indicated the significance of comparison between particle size and average size of porous media evoking lower permeability impairment and consequently lower damage.

Retention concentration at effluent was shown in Fig. 21. As shown, after 1.25 P.V capturing was started and its accelerating trend continues with decreasing slope after 4 P.V injections when the suspended concentration stabilized. This behaviour showed the dependency of flux reduction coefficient on jamming ratio that in case of stabilized flow, pore larger than the particle size due to decrease of flow in porous media.

The specified trend was observed in all other grid cells (Fig. 22).

In order to investigate the rate of retention throughout the core sample, retention concentration in each grid was reported for different time steps (Fig.23).

As observed, slope of retention concentration versus grid cell numbers was proportional to rate of retention which decreases as the front reached the outlet of core sample. To monitor size exclusion mechanism of mechanical formation damage dynamically, permeability decline curve was shown in Fig. 24 comparing the experimental and modelling results.

As observed, in first section of experimental data (P.V. lower than 0.5), inlet pressure increased and consequently permeability ratio decreased which is due to entry pressure of MgO NP's and can't be traced in model results.

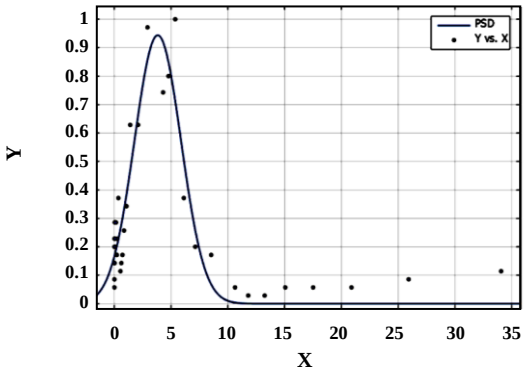


*Fig. 17: Tuned PSD curve of core sample with MATLAB fitting tools.*

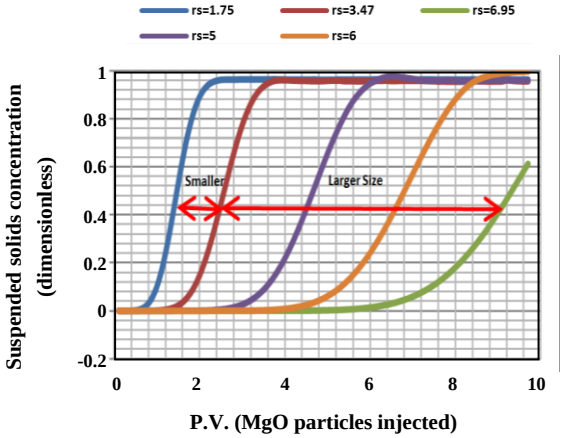


*Fig. 20: Suspension concentration at effluent throughout the injection time for different particle sizes.*

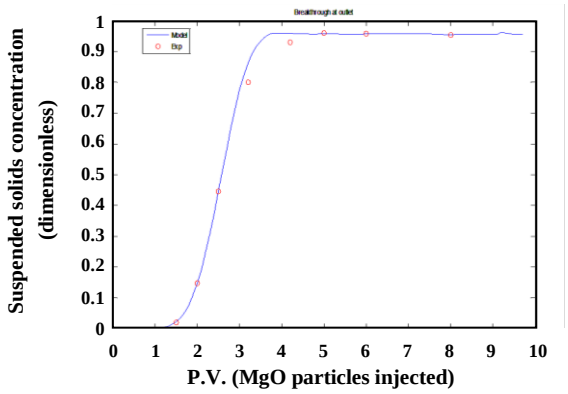


*Fig. 18: Suspension concentration at effluent throughout the injection time (Pa=0.7).*

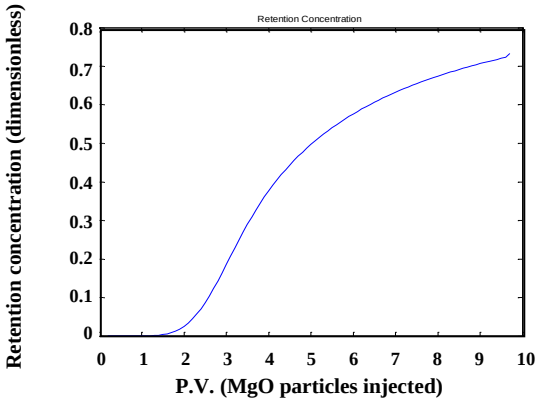


*Fig. 21: Retention concentration at effluent throughout the simulation time.*

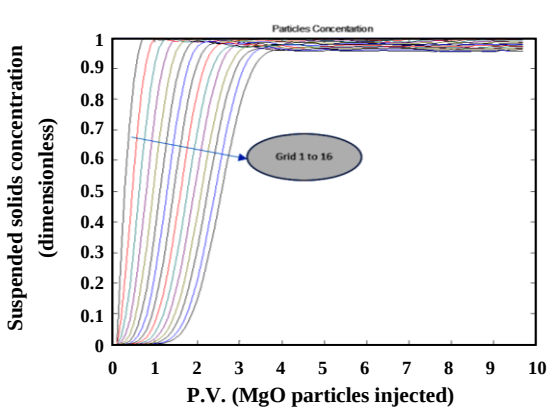


*Fig. 19: Suspension concentration at all grid cells throughout the simulation time.*

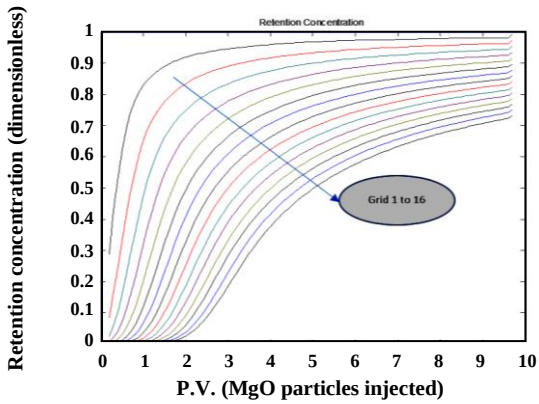


*Fig. 22: Retention concentration at all grid cells throughout the simulation time.*

Fig. 25 showed the trend of PSD changing dynamically. As observed, concentrations of pores larger than the injected particles (3.47 μm) do not change with time, since the pores allow particles to pass without being captured. Concentrations of all pores smaller than the particles ($r_p<r_s$) decreases with time monotonically [47].

## CONCLUSIONS

Experimental and modelling study was done to investigate the effect of PSD on mechanical formation damage due to size exclusion and the following results obtained:

- The experimental data show that the MgO NPs stabilized in anionic surfactant (accumar-3100) can be recommended as the suitable particles for design of stable particle movement experiment. Increase in surfactant concentration leads to decrease in droplet size was observed due to significant increase of interfacial area and reduction of interfacial energy which in turn reduces the interfacial tension denoting less coalescence of oil droplets and increase in stability of emulsion.
- Based on sensitivity analysis on capturing coefficient of particles, in case of core flooding in sandstone samples, best optimum value of capturing probability coefficient (pa) is 0.7 leading to the most consistent results of effluent concentrations with experimental measured at lab scale.
- Different order of magnitude in effluent concentration of particles regarding the particle sizes indicates the significance of comparison between particle size and average size of porous media as an indicator in design of injection water leading to lower formation damage.

**Acknowledgements**

The authors are grateful Research Institute of Petroleum Industry (RIPI), Iran.

**Numenclature**

| | |
|---|---|
| C | Suspended particle concentration distribution by sizes, L−4 |
| c | Total suspended particle concentration, L−3 |
| f | Fractional flow function, dimensionless |
| H | Pore concentration distribution, L−3 or L−4 |

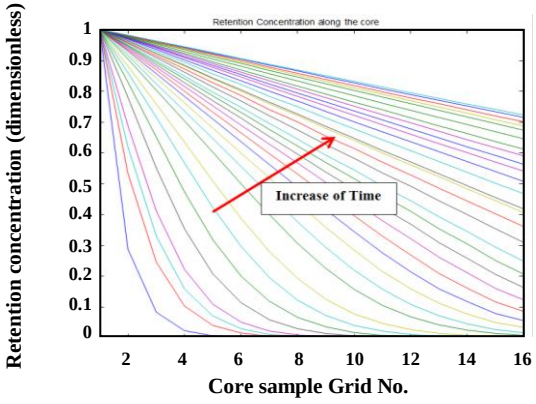


***Fig. 23: Retention concentration at all grid cells throughout the simulation time.***

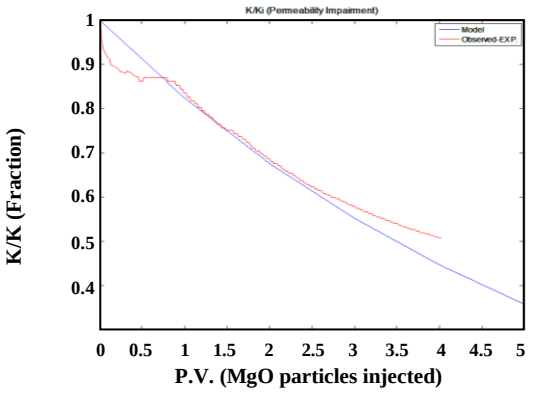


***Fig. 24: Comparison of experimental and modeling results of permeability decline due to size exclusion.***

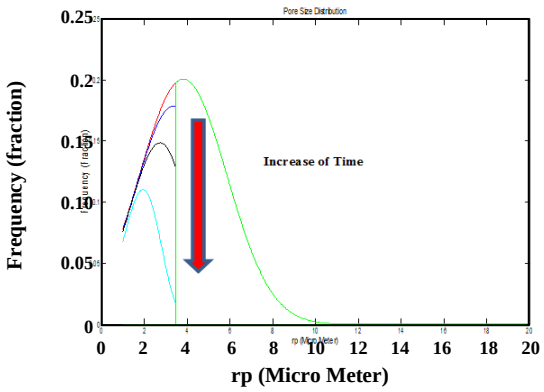


***Fig. 25: Dynamic change of PSD due to capturing of particles.***

| | |
|---|---|
| h | Total pore concentration (density), L −2 or L−3 |
| j | Jamming ratio, dimensionless |
| k(σ) | Absolute permeability, L2 |
| ka(σ) | Permeability of accessible part of the porous medium, L2 |
| kna(σ) | Permeability of inaccessible porous medium, L2 |
| kc(σ) | The total of pore accessible conductivities weighted with capture probability, L2 |
| l | Characteristic microscopic length, L |
| L | Length of the core, L |
| P | Pressure, M/LT |
| p(rs/rp) | Overall capture probability, dimensionless |
| pa(rs/rp) | Attachment capture probability, dimensionless |
| r | Size of a particle or of a pore, L |
| t | Time, T |
| U | Total velocity of the flux, L/T |
| v | Concentration front velocity in 1d filtration flow, L/T |
| x | Coordinate, L |
| λ-(σ ) | Filtration coefficient, $L^{-1}$ |
| λ(σ ) | Dimensionless filtration coefficient |
| ν(rs/rp) | Single pore flux reduction factor, dimensionless |
| σ | Volumetric concentration of captured particles, $L^{-3}$ |
| φ(x, t) | Porosity, dimensionless |
| φa(rs, x, t) | Accessible porosity for a particle of the size *rs* , dimensionless |
| φna(rs, x, t) | Inaccessible porosity for a particle |

*Received : June. 3, 2018 ; Accepted : Oct. 31, 2018*

**REFERENCES**

[1] Vetter O., Kandarpa V., Harouaka A., Prediction of Scale Problems Due to Injection of Incompatible Waters, *Journal of Petroleum Technology* , **34**: 273-284 (1982).

[2] Glossary S.O., Retrieved from the Internet< URL: https://www.glossary.oilfield.slb.com> Terms: *Electrical Stability Test, Electrical Resitivity, Invert Emulsion*, (2010).

[3] Moghadasi J., Jamialahmadi M., Müller-Steinhagen H., Sharif A., "Formation Damage Due to Scale Formation in Porous Media Resulting From Water Injection, Proceedings" - *SPE International Symposium on Formation Damage Control*, (2004)

[4] Civan F., "Reservoir Formation Damage", Gulf Professional Publishing, (2015).

[5] Valdya R., Fogler H., "Fines Migration and Formation Damage", *Journal of SPE Production Engineering*, **7**: 325-330 (1992).

[6] Meyers K., Skillman H., Herring G., Control of Formation Damage at Prudhoe Bay, Alaska, by Inhibitor Squeeze Treatment, *Journal of Petroleum Technology*, **37**(1): 019-011,034, (1985)

[7] Monaghan P., Salathiel R., Morgan B., Kaiser A., Laboratory Studies of in Sands Containing Clays, *SPE-1162-G*, (1959)

[8] Shaughnessy C., Kline W., EDTA Removes Formation Damage at Prudhoe Bay, *Journal of Petroleum Technology*, **35**: 1,783-781,791, (1983)

[9] Song W., Kovscek A.R., Direct Visualization of Pore-Scale Fines Migration and Formation Damage During Low-Salinity Waterflooding, *Journal of Natural Gas Science and Engineering*, **34**: 1276-1283, (2016)

[10] E. Lowry, M. Sedghi and L. Goual, Novel Dispersant for Formation Damage Prevention in $CO_2$: A Molecular Dynamics Study, *Journal of Energy & Fuels*, **30**: 7187-7195 (2016)

[11] Sheng J.J., Comparison of the Effects of Wettability Alteration and IFT Reduction on Oil Recovery in Carbonate Reservoirs, *Asia-Pacific Journal of Chemical Engineering*, **8** (1): 154-161 (2016).

[12] Betancur S., Carmona J.C., Nassar N.N., Franco C.A., Cortés F.B., Role of Particle Size and Surface Acidity of Silica Gel Nanoparticles in Inhibition of Formation Damage by Asphaltene in Oil Reservoirs, *Journal of Industrial & Engineering Chemistry Research*, **55**(21): 6122–6132 (2016).

[13] De Franceschi E., Castiñeiras T., Benedetto F., Funes A., Figini F., Economides M.J., Pipe Dope as a Source of Oil and Gas Formation Damage, *Journal of Natural Gas Science and Engineering*, **12**: 65-73 (2013).

[14] Khan H., Mirabolghasemi M., Yang H., Prodanovic M., DiCarlo D., Balhoff M., Gray K., "Comparative Study of Formation Damage due to Straining and Surface Deposition in Porous Media", *SPE International Symposium and Exhibition on formation Damage Control*, Lafayette, Louisiana, SPE-178930-MS, (2016).

[15] Moghadasi J., Jamialahmadi M., Müller-Steinhagen H., Sharif A., Izadpanah M., Motaei E., Barati R., "Formation Damage in Iranian Oil Fields", *International Symposium and Exhibition on Formation Damage Control*, (2002).

[16] Gray D., Rex R., "Formation Damage in Sandstones Caused by Clay Dispersion and Migration", *14th National Conference on Clay and Clay Minerals*, (1965).

[17] Khilar K.C., Fogler H.S., Migrations of Fines in Porous Media, *Journal of Springer Science & Business Media*, (1998).

[18] Juanes R., Spiteri E., Orr F., Blunt M., Impact of Relative Permeability Hysteresis on Geological $CO_2$ Storage, *Journal of Water Resources Research*, **42**: - (2006).

[19] El-Monier E.A., Nasr-El-Din H.A., A Study of Several Environmentally Friendly Clay Stabilizer, *SPE-142755-MS*, (2011)

[20] Habibi A., Al-Hadrami H.K.H., Al-ajmi A.M., Al-Wahaibi Y.M., Ayatollahi S., Effect of MgO Nanofluid Injection into Water Sensitive Formation to Prevent the Water Shock Permeability Impairment, *SPE-157106-MS*, (2012)

[21] Ju B., Fan T., Ma M., Enhanced Oil Recovery by Flooding with Hydrophilic Nanoparticles, *Journal of China Particuology*, **4**: 41-46 (2006).

[22] Torsater O., Engeset B., Hendraningrat L., Suwarno S., Improved Oil Recovery by Nanofluids Flooding: An Experimental Study, *SPE-163335-MS*, (2012)

[23] Karimi A., Fakhroueian Z., Bahramian A., Pour Khiabani N., Darabad J.B., Azin R., Arya S., Wettability Alteration in Carbonates Using Zirconium Oxide Nanofluids: EOR Implications, *Journal of Energy & Fuels*, **26**: 1028-1036 (2012).

[24] Xu B., Qiao Y., Park T., Tak M., Zhou Q., Chen X., A Conceptual Thermal Actuation System Driven by Interface Tension of Nanofluids, *Journal of Energy & Environmental Science*, **4**: 3632-3639 (2011).

[25] Zhang P., Shen D., Kan A.T., Tomson M.B., Synthesis and Laboratory Testing of a Novel Calcium-Phosphonate Reverse Micelle Nanofluid for Oilfield Mineral Scale Control, *Journal of RSC Advances*, **6**: 39883-39895 (2016).

[26] Kiani S., Mansouri Zadeh M., Khodabakhshi S., Rashidi A., Moghadasi J., Newly Prepared Nano Gamma Alumina and Its Application in Enhanced Oil Recovery: An Approach to Low-Salinity Water Flooding, *Journal of Energy & Fuels*, **30**: 3791-3797 (2016).

[27] Huang T., Crews J.B., Willingham J.R., Nanoparticles for Formation Fines Fixation and Improving Performance of Surfactant Structure Fluids, *IPTC-12414-MS*, (2008)

[28] Qu X., Alvarez P.J., Li Q., Impact of Sunlight and Humic Acid on the Deposition Kinetics of Aqueous Fullerene Nanoparticles (nC60), *Journal of Environmental Science & Technology*, **46**: 13455-13462 (2012).

[29] Wang Z., Yu T., Lin X., Wang X., Su L., Chemicals Loss and the Effect on Formation Damage in Reservoirs with ASP Flooding Enhanced oil Recovery, *Journal of Natural Gas Science and Engineering*, **33**: 1381-1389 (2016).

[30] Sheng J.J., A Comprehensive Review of Alkaline-Surfactant-Polymer (ASP) Flooding, *Asia-Pacific Journal of Chemical Engineering*, **9**: 471-489 (2014).

[31] Kuzmina L.I., Osipov Y.V., Modelling of Particles Retention in a Porous Soil, *Journal of Procedia Engineering*, **111**: 491-494 (2015).

[32] Chalk P., Gooding N., Hutten S., You Z., Bedrikovetsky P., Pore Size Distribution from Challenge Coreflood Testing by Colloidal Flow, *Journal of Chemical Engineering Research and Design*, **90**: 63-77 (2012).

[33] Farajzadeh R., "Produced Water Re-Injection (PWRI) An Experimental Investigation into Internal Filtration and External Cake Build up", Faculty of Civil Engineering and Geosciences, (2004).

[34] You Z., Osipov Y., Bedrikovetsky P., Kuzmina L., Asymptotic Model for Deep Bed Filtration, *Journal of Chemical Engineering Journal*, **258**: 374-385 (2014).

[35] Santos A., Barros P., Multiple Particle Retention Mechanisms during Filtration in Porous Media, *Journal of Environmental Science & Technology*, **44**: 2515-2521 (2010).

[36] Vahidi M., Rashidi A., Tavasoli A., Kiani S., Remarkable Enhancement of Convective Heat Transfer with Different Nanoparticles in N-Methyldiethanolamine Solution in Gas Sweetening Process, *Journal of International Communications in Heat and Mass Transfer*, **76**: 1-5 (2016).

[37] Dai C., Wang K., Liu Y., Li H., Wei Z., Zhao M., Reutilization of Fracturing Flowback Fluids in Surfactant Flooding for Enhanced Oil Recovery, *Journal of Energy & Fuels*, **29**: 2304-2311 (2015).

[38] Lee J.-H., Hwang K.S., Jang S.P., Lee B.H., Kim J.H., Choi S.U., Choi C.J., Effective Viscosities and Thermal Conductivities of Aqueous Nanofluids Containing Low Volume Concentrations of $Al_2O_3$ Nanoparticles, *International Journal of Heat and Mass Transfer*, **51**: 2651-2656 (2008).

[39] Alcázar-Vara L.A., Zamudio-Rivera L.S., Buenrostro-González E., Hernández-Altamirano R.l., V. Mena-Cervantes Y., Ramírez-Pérez J.F., Multifunctional Properties of Zwitterionic Liquids. Application in Enhanced Oil Recovery and Asphaltene Aggregation Phenomena, *Journal of Industrial & Engineering Chemistry Research*, **54**: 2868-2878 (2015).

[40] Wang L., Fan J., Nanofluids Research: Key Issues, *Nanoscale research letters*, **5**: 1241-1252 (2010).

[41] Klung H., Alexander L., Willey, "X-Ray Diffraction Procedures for Polycrystalline and Amorphous Materials", New York Publisher, EUA, 491, (1962).

[42] Sharma M., Yortsos Y., Fines Migration in Porous Media, *AIChE Journal*, **33**: 1636-1643 (1987).

[43] Bedrikovetsky P., Upscaling of Stochastic Micro Model for Suspension Transport in Porous Media, *Transport in Porous Media*, **75**: 335-369 (2008).

[44] Miranda R., Underdown D., Laboratory Measurement of Critical Rate: A Novel Approach for Quantifying Fines Migration Problems, *SPE 25432*, (1993).

[45] Parvazdavani M., Masihi M., Ghazanfari M.H., Monitoring the Influence of Dispersed Nano-Particles on Oil–Water Relative Permeability Hysteresis, *Journal of Petrol. Sci. Eng*, **124**: 222–231 (2014).

[46] Li S., Hendraningrat L., Torsaeter O., "Improved Oil Recovery by Hydrophilic Silica Nanoparticles Suspension: 2 Phase Flow Experimental Studies", In: *Proceedings of the IPTC*, (2013).

[47] Ahmadi M.A., Zendehboudi S., Shafiei A., James L., Nonionic Surfactant for Enhanced Oil Recovery from Carbonates: Adsorption Kinetics and Equilibrium, *Journal of Ind. Eng. Chem. Res*, **51**: 9894-9905 (2012).

[48] Meisam Kamalipour; Seyyed Ali AliMousavi Dehghani, Distinguishing Anhydrate and Gypsum Scale in Mixing Incompatible Surface and Ground Waters During Water Injection Process, *Iranian Journal of Chemistry and Chemical Engineering (IJCCE)*, **37**(1): 231-240 (2018).